Experimental polarization state tomography using optimal polarimeters

Alexander Ling,* Kee Pang Soh, Antía Lamas-Linares, and Christian Kurtsiefer
Department of Physics, National University of Singapore, 117542 Singapore, Singapore
(Received 14 March 2006; published 8 August 2006)

We report on the experimental implementation of a polarimeter based on a scheme known to be optimal for obtaining the polarization vector of ensembles of spin-$\frac{1}{2}$ quantum systems and the alignment procedure for this polarimeter. We also show how to use this polarimeter to estimate the polarization state for identically prepared ensembles of single photons and photon pairs and extend the method to obtain the density matrix for generic multiphoton states. State reconstruction and performance of the polarimeter is illustrated by actual measurements on identically prepared ensembles of single photons and polarization entangled photon pairs.

DOI: 10.1103/PhysRevA.74.022309 PACS number(s): 03.67.−a, 03.65.Wj, 07.60.Fs, 42.25.Ja

I. INTRODUCTION

Many promising applications in quantum information (e.g., quantum computation and quantum communication) demand accurate state estimation. For many of them it is compelling to implement state estimation techniques that are both fast and consume as few copies of the state as possible. Research in improving the efficiency of quantum state estimation techniques is an area of active theoretical study [1–7] with much focus on spin-$\frac{1}{2}$ systems (qubits). Experimental reports on state estimation are fewer [8], partly because many schemes call for a joint measurement of an ensemble of qubits which is not always possible to implement.

One way to realize qubits experimentally is to use single photons and consider their polarization degree of freedom, as this can be described by a two-dimensional Hilbert space. Estimating the polarization state of an ensemble of single photons (called polarimetry in classical optics) is equivalent to estimating the state of the qubit ensemble. This makes efficient polarimetry interesting to quantum information.

Polarimetry that uses the least number of measurement outcomes is said to be minimal. Minimal polarimetry techniques in classical optics have been known for a long time, and a lot of work in their optimization has been done [9–13]. While these classical methods perform well in estimating the polarization state for single-photon ensembles in the limit of large numbers, their performance in the regime of extremely low light intensity (single-photon level) was uncertain and it was not obvious how to use them in estimating nonclassical states of light. For this reason, progress in polarimetry at the single-photon limit will assist in many areas, including characterization of faint sources of light, classical ellipsometry [9], advanced quantum key distribution protocols [14–16], and studies of the fundamental aspects of quantum theory [17].

In discriminating between different estimation techniques we distinguish between methods that are minimal and those that are minimal *and* optimal [3,7]: optimal methods have the best asymptotic efficiency in determining an unknown state when averaged over all possible input states. This can be used for an operational definition of minimal and optimal state estimation for ensembles of prepared quantum systems. It is the technique that provides the best improvement to our estimated state for each additional copy taken from the ensemble. Recently Řeháček *et al.* proposed such a method for state estimation of polarization-based single qubits [7], which can be viewed as an extension of classical techniques [10,11,18] to quantum systems.

In this paper we address the experimental problem of implementing the optimal state estimation method described in [7] by using a complete four-output polarimeter with no moving parts. We describe that polarimeter in Sec. II by reviewing the theory of optimal polarization state estimation and explain our implementation. In Sec. III polarization state estimation of multiphoton states is addressed. In Sec. IV we elaborate on the alignment procedure to make the polarimeter perform optimally. Experimental state reconstruction on ensembles of single photons and photon pairs with high fidelity will be illustrated in Secs. V and VI.

II. STATE ESTIMATION USING THE OPTIMAL POLARIMETER

The polarization state of light can be characterized using the three Stokes parameters S_1, S_2, and S_3, possibly augmented by an intensity S_m. Together they form a Stokes vector $\vec{S}$ and, when normalized, it is written as $\vec{S}=(1,S_1/S_m,S_2/S_m,S_3/S_m)$. A *reduced* Stokes vector $\vec{S}_r=(S_1,S_2,S_3)/S_m$ identifies a point in the Poincaré sphere (in this paper reduced Stokes vectors are denoted by an r subscript) [19].

A minimal scheme of estimating the Stokes vector requires exactly four detector readings, which corresponds to finding the overlap of the unknown Stokes vector with four noncoplanar vectors that define a tetrahedron in the Poincaré sphere (Fig. 1). These four noncoplanar vectors define four measurement operators B_j that govern the detector readings and form a set of complete positive operator value measurements (POVM's) [20]. The tetrahedron geometry defines the largest volume that can be enclosed by a vector quartet in the Poincaré sphere, making it the optimal estimation technique when using four POVM's [11,21]. Such a state estimation technique is also unbiased in the asymptotic limit because

*Electronic address: phylej@nus.edu.sg; http://www.quantumlah.org

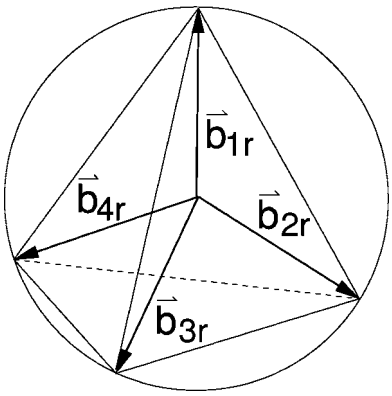

FIG. 1. Four (reduced) Stokes vectors in the Poincaré sphere that form a tetrahedron define the optimal POVM operators used for polarization state estimation. The tetrahedron gives the largest volume encompassable by a vector quartet in the sphere, making it the optimal measurement when using four POVM's.

the total distance of any vector in the Poincaré sphere to all four POVM vectors depends only on the vector's magnitude. In other words, the orientation of the unknown vector does not affect the accuracy with which it is estimated [7].

We shall denote the tetrahedron's reduced Stokes vectors by $\vec{b}_{1r}$, $\vec{b}_{2r}$, $\vec{b}_{3r}$, and $\vec{b}_{4r}$ as shown in Fig. 1 and write their corresponding normalized vectors as $\vec{b}_1$, $\vec{b}_2$, $\vec{b}_3$, and $\vec{b}_4$. Each measurement operator B_j may be expressed as

$$B_j = \frac{1}{4}(\vec{b}_j \cdot \vec{\sigma}), \tag{1}$$

where $\vec{\sigma}=(\sigma_0,\sigma_1,\sigma_2,\sigma_3)$, σ_0 being the unit matrix and $\sigma_{1,2,3}$ the Pauli matrices.

In an experiment we associate each operator B_j with a detector b_j. The average intensity falling on detector b_j is denoted as I_j. Thus expectation values of the tetrahedron operators are related to detected intensities as follows:

$$\frac{I_j}{I_t} = \langle B_j \rangle = \frac{1}{4}(\vec{b}_j \cdot \vec{S}), \tag{2}$$

with

$$I_t = \sum_{j=1}^{4} I_j.$$

Writing the intensities as a vector $\vec{I}=(I_1,I_2,I_3,I_4)/I_t$ gives us the Stokes vector

$$\vec{I} = \Pi \cdot \vec{S} \Leftrightarrow \vec{S} = \Pi^{-1} \cdot \vec{I}, \tag{3}$$

where Π is referred to as the instrument matrix. Each row of this matrix is composed from a vector $\vec{b}_j$. One possible instrument matrix of the ideal polarimeter is

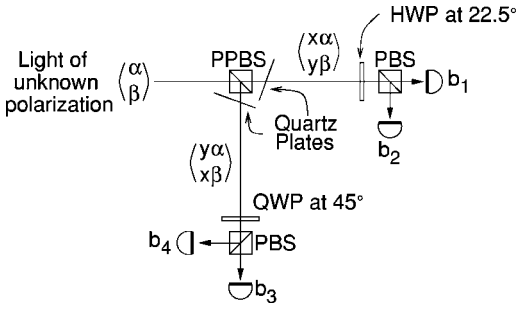

FIG. 2. Practical implementation of the tetrahedron polarimeter that achieves the ideal instrument matrix. Each detector b_j is associated to the tetrahedron vector $\vec{b}_j$. The partially polarizing beam splitter (PPBS) separates incoming light according to polarization, and quartz plates remove unwanted phase shifts. Light leaving the PPBS is passed through wave plates and polarizing beam splitters (PBS) to be projected on two different bases (±45° basis for transmitted light and the circular basis for reflected light).

$$\Pi = \frac{1}{4}\begin{pmatrix} 1 & \sqrt{\frac{1}{3}} & \sqrt{\frac{2}{3}} & 0 \\ 1 & \sqrt{\frac{1}{3}} & -\sqrt{\frac{2}{3}} & 0 \\ 1 & -\sqrt{\frac{1}{3}} & 0 & -\sqrt{\frac{2}{3}} \\ 1 & -\sqrt{\frac{1}{3}} & 0 & \sqrt{\frac{2}{3}} \end{pmatrix}. \tag{4}$$

Experimental realization of this instrument matrix is achieved by the polarimeter shown in Fig. 2. The first component of the polarimeter is a partially polarizing beam splitter (PPBS) that has a particular amplitude splitting ratio for incoming light, most easily determined using Jones vector notation for polarization. The amplitude division coefficients of the PPBS, x and y, obey energy conservation $|x^2|+|y^2|=1$. The PPBS takes horizontally polarized (H) light $\binom{1}{0}$ to the polarizations $\binom{x}{0}$ and $\binom{y}{0}$ in the transmitted and reflected arms, respectively, and vertically (V) polarized light $\binom{0}{1}$ to $\binom{0}{y}$ in transmission and $\binom{0}{x}$ in reflection.

If we project light in the transmitted arm of the PPBS on the ±45° polarization basis and light in the reflected arm onto the left and right circular polarization bases, the tetrahedral arrangement of the vectors $\vec{b}_j$ is ensured with the following relations:

$$x^2 = \frac{1}{2} + \frac{1}{2\sqrt{3}}, \quad y^2 = \frac{1}{2} - \frac{1}{2\sqrt{3}}. \tag{5}$$

Detailed steps are given in the Appendix .

Partially polarized light can be described using a density matrix (or coherency matrix). If we write the entries of the density matrix as a column vector $\vec{\rho}$, we can determine them from the Stokes vector [22] using the following transformation:

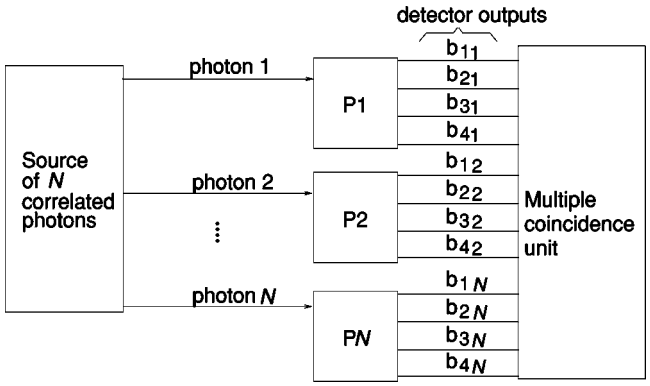

FIG. 3. Scheme for estimating the polarization state of an ensemble of N-correlated photons using N polarimeters $(P1,P2,\ldots,PN)$. A multiple-coincidence circuit identifies the 4^N possible coincidence combinations. For photon pairs $(N=2)$, two polarimeters are used, giving 16 possible coincidence combinations. Several copies of the state are processed, giving a coincidence pattern used in estimating the polarization state of the ensemble.

$$\vec{\rho} = \frac{1}{2}\Gamma_1 \cdot \vec{S} = \frac{1}{2}\begin{pmatrix} 1 & 1 & 0 & 0 \\ 0 & 0 & 1 & i \\ 0 & 0 & 1 & -i \\ 1 & -1 & 0 & 0 \end{pmatrix} \cdot \vec{S}. \tag{6}$$

The columns of the matrix Γ_1 are the Pauli operators written as column vectors $\Gamma_1=(\vec{\sigma}_0,\vec{\sigma}_1,\vec{\sigma}_2,\vec{\sigma}_3)$. The matrices B^{-1} and Γ_1 can be combined into a single matrix

$$T := \frac{1}{2}\Gamma_1 \Pi^{-1} \Rightarrow \vec{\rho} = T \cdot \vec{I}, \tag{7}$$

which might be referred to as a tomography matrix as it directly relates the detected intensities to the density matrix of the state.

III. POLARIZATION STATE TOMOGRAPHY FOR ENSEMBLES WITH MULTIPHOTONS

The instrument matrix scheme above can be extended to perform polarization state tomography on ensembles of multiphoton states. James *et al.* [8] have described a similar state estimation method. We follow their approach but use our optimal and instrumentally motivated measurement operators, thereby reducing any ambiguity over the choice of operators.

The simplest multiphoton system is a photon pair detected by testing for coincidence in the detection time of their component photons. In our measurement process each member of the photon pair is passed through a polarimeter. Given two polarimeters 1 and 2, each with four detectors b_{i_1} and b_{i_2}, respectively $(i_1,i_2=0,1,2,3)$, we will have 16 possible coincidence combinations between the detectors (see Fig. 3). Each coincidence rate is governed by an operator composed from the individual detectors' measurement operators. If we denote again the measurement operator of detectors b_{i_1} and b_{i_2} as B_{i_1} and B_{i_2} and the coincidence count between them as c_{i_1,i_2}, we can express the coincidence rates as a linear function of a two-photon polarization state vector S_2:

$$\frac{c_{i_1,i_2}}{c_t} = \langle B_{i_1} \otimes B_{i_2} \rangle = \left(\frac{1}{4}\vec{b}_{i_1} \otimes \frac{1}{4}\vec{b}_{i_2}\right) \cdot \vec{S}_2, \tag{8}$$

with

$$c_t = \sum_{i_1,i_2=1}^{4} c_{i_1,i_2}.$$

Here, $\vec{S}_2$ is the Stokes vector equivalent for a two-photon system [8] and c_t is the total number of observed coincidences. We now have the set of measurement operators governing the coincidence pattern. The 16 coincidences c_{i_1,i_2} can be written in column vector format $\vec{C}_2=(c_{1,1},c_{1,2},\ldots,c_{4,4})$. If we define the two-polarimeter instrument matrix as Π_2, we obtain an instrument response analogous to (3):

$$\vec{C}_2 = \Pi_2 \cdot \vec{S}_2 \Leftrightarrow \vec{S}_2 = \Pi_2^{-1} \cdot \vec{C}_2. \tag{9}$$

Thus we obtain the density matrix of the two-photon state by constructing the analogous two-photon expression for Eq. (6):

$$\vec{\rho}_2 = \frac{1}{2^2}\Gamma_2 \cdot \vec{S}_2 = T_2 \cdot \vec{C}_2. \tag{10}$$

Each column of Γ_2 is the product of two Pauli operators $\sigma_{i_1} \otimes \sigma_{i_2}$ $(i_1,i_2=0,1,2,3)$ written in column vector format, and T_2 is the tomography matrix for the two-photon state.

It is now straightforward to generalize this concept to obtain the density matrix for states of N correlated photons. Using N polarimeters, we obtain the pattern of N-fold coincidences to build up the coincidence vector $\vec{C}_N$ which is used to find the N-photon Stokes vector and density matrix:

$$\vec{S}_N = \Pi_N^{-1} \cdot \vec{C}_N, \tag{11}$$

$$\vec{\rho}_N = \frac{1}{2^N}\Gamma_N \cdot \vec{S}_N = T_N \cdot \vec{C}_N. \tag{12}$$

Each row of the instrument matrix Π_N is given by $\left(\frac{1}{4}\vec{b}_{i_1} \otimes \frac{1}{4}\vec{b}_{i_2} \cdots \otimes \frac{1}{4}\vec{b}_{i_N}\right)$ and each column of Γ_N is the product of N Pauli matrices $\sigma_{i1} \otimes \sigma_{i_2} \cdots \otimes \sigma_{i_n}$ $(i_n=0,1,2,3$ and $n=1,2,\ldots,N)$. This generalized approach will work for all four-detector polarimeters in multiphoton analysis schemes (Fig. 3). We note that—although the polarimeters are optimal for estimating single qubit states—it is an open question if the scheme above is optimal in estimating multiphoton systems.

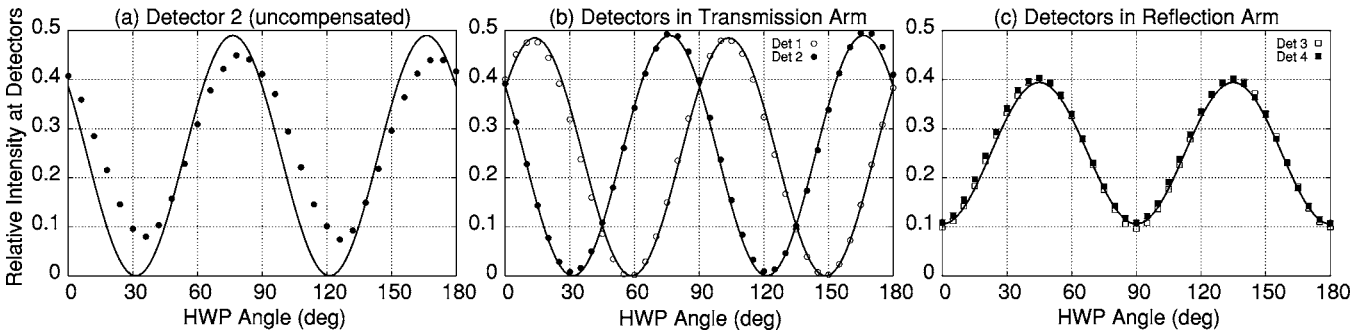

FIG. 4. Instrument response of the polarimeter to linearly polarized light. The data points show the variation in relative intensity at each detector with respect to the angle of the half-wave plate (HWP) in the polarization state preparation. The solid lines show the expected intensity modulation for an ideal device for each HWP setting [(13)], scaled for appropriate detector efficiencies. Error bars are smaller than the point markers. Panel (a) shows the relative intensity at detector 2 without compensation plates. Panels (b) and (c) are taken with compensation for phase shifts. The oscillation in (a) is out of phase and also of lower amplitude compared to the phase-corrected behavior of detector 2 in panel (b). Plots in (c) shows a lower amplitude because light in the reflected arm is not projected on a linear polarization basis.

IV. PHASE CORRECTION AND POLARIMETER CALIBRATION

A. Removing unwanted phase shifts

In the presented polarimeter, an ideal PPBS has the nominal beam splitting ratio (5) and also rotates the polarization state of light leaving the beam splitter into the correct polarization basis [12]. Such beam splitters, however, are not easily available and their design is the focus of active research [23]. We therefore use beam splitters with only the nominal intensity splitting ratio.

A PPBS without a phase shift diverts light in state $-\vec{b}_{jr}$ (which is conjugate to a tetrahedron vector $\vec{b}_{jr}$) from detector b_j. General beam splitters, however, lack this phase-preserving property. The result is that input of conjugate states $-\vec{b}_{jr}$ does not stop light from reaching the associated detectors. This suggests an easy alignment method for correcting any unwanted phase shifts with birefringent compensation plates.

For phase correction we first prepare high-quality H-polarized light using polarizers of extinction ratio 10^5. With one subsequent half-wave plate (HWP) and one quarter-wave plate (QWP) we can then prepare any polarization state on the surface of the Poincaré sphere. Compensator plates (0.5-mm-thick quartz) mounted on rotating stages were placed at each output arm of the PPBS, and light with a conjugate polarization state was sent to the polarimeter. For each polarization state $-\vec{b}_{jr}$ the compensator in the relevant output arm was rotated until the detector b_j received no light. Two input states (one for each output arm) were sufficient to compensate for the unwanted phase shifts.

We verified the compensated polarimeter behavior with linearly polarized light prepared using only the polarizer and HWP (this reduces preparation errors due to residual errors in the QWP). The prepared states have a Stokes vector of the form $(1, \cos 4\psi, \sin 4\psi, 0)$, where ψ is the angle of the HWP, so the normalized response of detector 1, for example, will be

$$I_1 = 1 + \sqrt{\frac{1}{3}} \cos 4\psi + \sqrt{\frac{2}{3}} \sin 4\psi. \tag{13}$$

Passively quenched silicon avalanche photodiodes were used as detectors allowing us to perform photon counting. The number of photons accumulated at each detector output was noted for each angle of the HWP. The results are shown in Fig. 4.

The results show that the response of the compensated polarimeter is very close to ideal. The extrema of our measured intensities are less than 1° (of HWP angle) away from their nominal positions. This means that our actual measurement vectors are pointing in the same direction as the ideal tetrahedron vectors, although their magnitudes will be different due to imbalanced detection efficiencies. While this renders the asymptotic efficiency of our polarimeter less than ideal, it still represents the optimal setup for the collection efficiencies we can achieve. In other words, we are maximizing the volume defined by our experimental POVM vectors [21].

This measurement result is limited by the accuracy of our rotation controllers. Our wave plates are mounted on rotary motors with an accuracy of 0.3°. The polarizing beam splitters in the output arms have an extinction ratio of 10^4 and the wave plates' optical path lengths differ from their nominal values by less than 2%.

B. Calibrating the polarimeter

We calibrate the instrument matrix of this polarimeter to account for all residual phase shifts and coupling inefficiencies. A general calibration technique for four detector polarimeters ("equator-pole method") was described by Azzam *et al.* [18]. Incidentally, the phase dependence measurement shown in Fig. 4 was an essential part of this calibration.

Using this technique we are able to find the correction terms needed to be made to our ideal instrument matrix. A typical corrected instrument matrix is

$$\Pi_c = \frac{1}{4}\begin{pmatrix} 0.962 & 1.051\sqrt{\frac{1}{3}} & 0.920\sqrt{\frac{2}{3}} & 0.005 \\ 0.991 & 1.031\sqrt{\frac{1}{3}} & -0.956\sqrt{\frac{2}{3}} & -0.005 \\ 1.010 & -1.045\sqrt{\frac{1}{3}} & 0.005 & -0.945\sqrt{\frac{2}{3}} \\ 1.032 & -1.009\sqrt{\frac{1}{3}} & 0.029 & 1.011\sqrt{\frac{2}{3}} \end{pmatrix}.$$

The uncertainty for each of the correction terms above is on the order of 0.002. We see that the deviation from entries in the ideal instrument matrix (4) is on the order of a few percent.

The phase correction and calibration steps presented above must take into account the wavelength of the input light because optical elements are specified to perform only within a certain bandwidth. The polarimeter was built to study the polarization state of light coming from a spontaneous parametric down-conversion (SPDC) source [24] with a spectral bandwidth of 4.740 ± 0.014 nm centered around 702 nm. The same light source was used for phase correction and polarimeter calibration and the experiments described in the remaining sections.

V. EXPERIMENTAL STATE TOMOGRAPHY FOR ENSEMBLES OF SINGLE PHOTONS

The ability of the tetrahedron polarimeter to estimate polarization states without bias was tested by preparing a set of pure polarization states equally distributed over the Poincaré sphere. In this way we could better identify regions that suffer poor state estimation (if any).

Computer-controlled motors were used to rotate wave plates (after a H filter) in preparing the set of polarization states. The Stokes vector of a pure polarization state can be expressed as $\vec{S}=(1,\cos 2\delta \cos 2[\psi+\delta],-\cos 2[\psi+\delta]\sin 2\delta, -\sin 2[\psi+\delta])$, where δ and ψ are the QWP and HWP angles, respectively. Thus any set of coordinates (characterized by the polar and azimuthal angles) on the Poincaré sphere can be expressed in terms of the wave plate angles.

For each set of angles, the detectors accumulated photon detection events for 1 s giving a particular vector $\vec{I}$ from which an estimated Stokes vector $\vec{S}_e$ and probability density matrix ρ_e can be obtained via Eqs. (3) and (6). To calculate the distance of the estimated state from the (ideal) prepared state ρ_i $(\vec{S}_i)$, we use the Uhlmann fidelity, defined as $(\mathrm{tr}[\sqrt{\sqrt{\rho_i}\rho_e\sqrt{\rho_i}}])^2$ [25,26]. For pure states this quantity reduces to the overlap of their Stokes vectors $\frac{1}{2}(\vec{S}_i \cdot \vec{S}_e)$.

The fidelity was mapped to the appropriate polar and azimuthal coordinates on the Poincaré sphere (Fig. 5); linear polarization states correspond to a polar angle of 0°. The average fidelity for the whole map is 99.8% with a minimum fidelity of $98.4\% \pm 0.9\%$ (the cumulative photon count per point is approximately 2000). There are no systematic areas of low fidelity even when wedge errors in the state preparation wave plates cause count rates to drop. This indicates that the polarimeter estimates all pure polarization states equally well.

Fidelity does not distinguish between errors introduced in state preparation from errors in the state estimation process. Therefore we have characterized our state preparation apparatus independently and are confident that their contribution to the error in calculated fidelity above is on the order of $\pm 0.01\%$. Thus we assign the residual difference in fidelity to imperfections in the detection apparatus.

VI. EXPERIMENTAL STATE TOMOGRAPHY FOR A TWO-PHOTON ENSEMBLE

We will now illustrate how to use two polarimeters to perform polarization state tomography on a two-photon state generated from an SPDC source. First, two polarimeters were correctly aligned and after calibration their instrument matrices were found to be

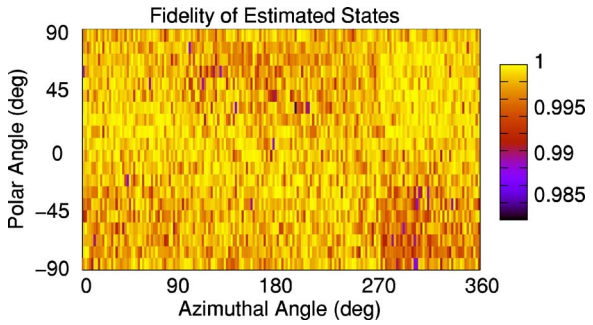

FIG. 5. (Color online) A set of polarization states $(\vec{S}_i)$ equally distributed over the Poincaré sphere surface was generated; photons from each of these states were sent to the polarimeter, from which an estimated state $(\vec{S}_e)$ is obtained. The figure shows the fidelity of the estimated state to the prepared state, $\frac{1}{2}(\vec{S}_e \cdot \vec{S}_i)$. It is roughly constant over the Poincaré sphere, showing that the polarimeter is an unbiased polarization state estimator.

$$\frac{1}{4}\begin{pmatrix} 0.903 & 0.927\sqrt{\frac{1}{3}} & 0.9997\sqrt{\frac{2}{3}} & -0.041 \\ 1.124 & 1.135\sqrt{\frac{1}{3}} & -1.014\sqrt{\frac{2}{3}} & 0.0602 \\ 0.995 & -1.079\sqrt{\frac{1}{3}} & 0.001 & 0.913\sqrt{\frac{2}{3}} \\ 0.978 & -0.983\sqrt{\frac{1}{3}} & 0.003 & -0.936\sqrt{\frac{2}{3}} \end{pmatrix}$$

and

$$\frac{1}{4}\begin{pmatrix} 1.074 & 1.171\sqrt{\frac{1}{3}} & 0.913\sqrt{\frac{2}{3}} & -0.082 \\ 0.983 & 0.8804\sqrt{\frac{1}{3}} & -1.044\sqrt{\frac{2}{3}} & 0.004 \\ 1.082 & -1.172\sqrt{\frac{1}{3}} & 0.001 & -0.9625\sqrt{\frac{2}{3}} \\ 0.862 & -0.88\sqrt{\frac{1}{3}} & -0.002 & 0.867\sqrt{\frac{2}{3}} \end{pmatrix}.$$

We then arranged for the SPDC source to generate photon pairs that are detected as a maximally entangled Bell state $|\Psi^+\rangle$. Bell states created via SPDC are typically characterized by a polarization correlation experiment, from which a visibility value can be obtained [24]. The visibility measured in the HV and ±45° basis was above 97.7% ±2%; such a high value is usually taken as evidence of a high degree of entanglement.

The photon pairs were passed through the polarimeters and the pattern of coincidences between them was observed. The 16 observed coincidence rates (collected using the scheme similar to [27]) make up the coincidence vector $\vec{C}$=(21444, 1505, 24104, 26002, 979, 24716, 23210, 22447, 21661, 30752, 24061, 268, 19010, 23692, 339, 17695).

Using this vector with Eqs. (9) and (10) we obtain the density matrix whose real components are

$$\mathrm{Re}[\rho] = \begin{pmatrix} -0.002 & -0.01 & -0.03 & -0.024 \\ -0.01 & 0.506 & 0.485 & 0.025 \\ -0.03 & 0.485 & 0.498 & 0.009 \\ -0.024 & -0.024 & 0.009 & -0.003 \end{pmatrix},$$

while the magnitude of the imaginary components are below a value of 0.04 (see Fig. 6).

The uncertainty in each of the above terms is on the order of 0.011. The Uhlmann fidelity of this state to the ideal $|\Psi^+\rangle$ state was found to be 0.990±0.014. Error bars in all cases were computed by numerical derivation and propagated Poissonian counting noise. The propagated error bars result in an estimated density matrix compatible with the ideal $|\Psi^+\rangle\langle\Psi^+|$ state.

VII. CONCLUSION

In this paper we have illustrated a simple alignment procedure for optimizing the tetrahedron polarimeter. Phase shifts introduced by a commercially available PPBS were easily corrected by phase compensation plates in the output arms. The response of the compensated polarimeter was measured over a dense sampling of states on the Poincaré sphere and found to be similar to that of an ideal device. This shows that beam splitters need only have the nominal intensity splitting ratio, making optimal polarimeters more accessible.

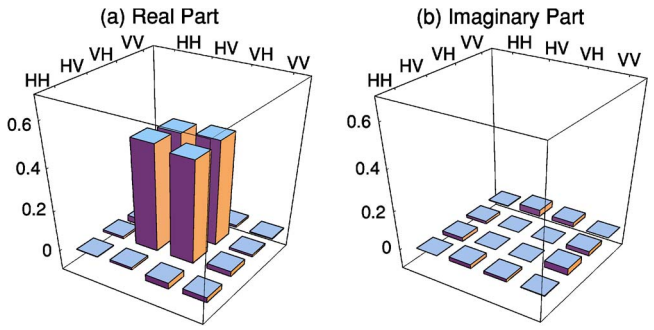

FIG. 6. (Color online) The density matrix of a Bell state $|\Psi^+\rangle\langle\Psi^+|$ obtained by linear reconstruction from photon pairs.

We also described an instrumentally motivated method for constructing the measurement operators governing light distribution to each output of the polarimeter. This instrument-based approach also allows a convenient generalization to obtain measurement operators governing multiphoton coincidences. These operators can then be applied to the linear reconstruction of multiphoton Stokes vectors and their density matrices.

Optimal polarimeters were then used for estimating the polarization state of experimentally prepared ensembles of single photons and photon pairs in a Bell state. The estimated states were evaluated by computing their fidelity to the (ideal) prepared states. We found an average fidelity above 99.8% in all our experiments. Thus we have built and demonstrated the use of optimal four-output polarimeters in multiphoton polarization state tomography.

While preparing this document, it came to our attention that a similar four output polarimeter was suggested independently in a recent paper [17].

ACKNOWLEDGMENTS

We would like to thank Ivan Marcikic, Berge Englert, and Janet Anders for helpful discussions. This work was supported by DSTA Grant No. R-394-000-019-422 and A*Star Grant No. R-144-000-071-305.

APPENDIX

To derive the intensity splitting ratio of the PPBS, we first express the polarization states are expressed using Jones vectors unless we are describing the tetrahedron vectors $\vec{b}_j$. The tetrahedron (Stokes) vectors $\vec{b}_{j,k}$ have the scalar product property

$$\vec{b}_j \cdot \vec{b}_k = \frac{2}{3} + \frac{4}{3}\delta_{jk}. \quad \text{(A1)}$$

Recalling the parameters of the intensity splitting ratio of the PPBS, x and y, we see that a general input polarization state $\binom{\alpha}{\beta}$ leads to the polarizations $\binom{x\alpha}{y\beta}$ and $\binom{y\alpha}{x\beta}$ in the transmitted and reflected arms of the PPBS, respectively. In our polarimeter, light leaving the arms of the PPBS must be analyzed in two different polarization bases. Two orthogonal vectors that form a basis may be expressed as $\binom{\cos\theta}{e^{i\phi}\sin\theta}$ and $\binom{-e^{-i\phi}\sin\theta}{\cos\theta}$. This leads, for example, to the normalized light intensity falling on detector b_1:

$$I_1/I_t = |\alpha x \cos\theta + \beta y e^{-i\phi}\sin\theta|^2. \tag{A2}$$

We choose a different measurement basis for detectors 3 and 4: for example, light reaching detector 3 is

$$I_3/I_t = |\alpha y \cos\theta' + \beta x e^{-i\phi'}\sin\theta'|^2. \tag{A3}$$

Using the vector $\vec{b}_1$ as an example, Eq. (2) allows us to express the operator B_1 in terms of the measurement basis to fulfill Eq. (A2):

$$\langle B_1\rangle = |\alpha x \cos\theta + \beta y e^{-i\phi}\sin\theta|^2 \tag{A4}$$

$$= \left|\begin{pmatrix} x\cos\theta & y e^{-i\phi}\sin\theta\end{pmatrix}\begin{pmatrix}\alpha\\ \beta\end{pmatrix}\right|^2. \tag{A5}$$

The following choice of B_1 fulfills this condition:

$$B_1 = \begin{pmatrix} x\cos\theta \\ y\sin\theta e^{i\phi}\end{pmatrix}(x\cos\theta \quad y\sin\theta e^{-i\phi}). \tag{A6}$$

Since the tetrahedron can be oriented arbitrarily we choose for convenience to measure the 45° linear polarization basis ($\theta=\pi/4$, $\phi=0$) in the transmitted arm and the circular polarization basis ($\theta'=\pi/4$ $\phi'=\pi/2$) in the reflected arm. This reduces the measurement operators to only the beam splitting parameters x and y,

$$\left.\begin{matrix}B_1\\ B_2\end{matrix}\right\} = \frac{1}{2}\begin{pmatrix} x^2 & \pm xy\\ \pm xy & y^2\end{pmatrix}, \qquad \left.\begin{matrix}B_3\\ B_4\end{matrix}\right\} = \frac{1}{2}\begin{pmatrix} y^2 & \mp ixy\\ \pm ixy & x^2\end{pmatrix},$$

which together with Eq. (2) allows us to express all tetrahedron vectors in terms of x and y:

$$\left.\begin{matrix}\vec{b}_1\\ \vec{b}_2\end{matrix}\right\} = \begin{pmatrix} 1\\ x^2-y^2\\ \pm 2xy\\ 0\end{pmatrix}, \qquad \left.\begin{matrix}\vec{b}_3\\ \vec{b}_4\end{matrix}\right\} = \begin{pmatrix} 1\\ y^2-x^2\\ 0\\ \mp 2xy\end{pmatrix}. \tag{A7}$$

From Eq. (A1), we can write

$$\vec{b}_1\cdot\vec{b}_2 = \frac{2}{3}, \quad \vec{b}_1\cdot\vec{b}_3 = \frac{2}{3}. \tag{A8}$$

This allows us to obtain an equation in x alone:

$$36x^8 - 24x^4 + 1 = 0. \tag{A9}$$

The last equation gives two solution sets; we choose the set where $x^2=\frac{1}{2}+\frac{1}{2\sqrt{3}} \Rightarrow y^2=\frac{1}{2}-\frac{1}{2\sqrt{3}}$.

[1] S. Massar and S. Popescu, Phys. Rev. Lett. **74**, 1259 (1995).
[2] R. Derka, V. Bužek, and A. K. Ekert, Phys. Rev. Lett. **80**, 1571 (1998).
[3] J. I. Latorre, P. Pascual, and R. Tarrach, Phys. Rev. Lett. **81**, 1351 (1998).
[4] R. D. Gill and S. Massar, Phys. Rev. A **61**, 042312 (2000).
[5] R. Schack, T. A. Brun, and C. M. Caves, Phys. Rev. A **64**, 014305 (2000).
[6] E. Bagan, M. Baig, R. Muñoz-Tapia, and A. Rodriguez, Phys. Rev. A **69**, 010304(R) (2004).
[7] J. Řeháček, B.-G. Englert, and D. Kaszlikowski, Phys. Rev. A **70**, 052321 (2004).
[8] D. F. V. James, P. G. Kwiat, W. J. Munro, and A. G. White, Phys. Rev. A **64**, 052312 (2001).
[9] R. M. A. Azzam, in *Handbook of Optics*, 2nd ed., edited by M. Bass, E. W. van Stryland, D. R. Williams, and W. L. Wolfe (McGraw-Hill, New York, 1995), Vol. II, Chap. 27.
[10] A. Ambirajan and D. C. Look, Jr., Opt. Eng. (Bellingham) **34**, 1651 (1995).
[11] A. Ambirajan and D. C. Look Jr., Opt. Eng. (Bellingham) **34**, 1656 (1995).
[12] R. Azzam and A. De, J. Opt. Soc. Am. A **20**, 955 (2003).
[13] D. S. Sabatke, M. R. Descour, E. L. Dereniak, W. C. Sweatt, S. A. Kemme, and G. S. Phipps, Opt. Lett. **25**, 802 (2000).
[14] D. Bruß, M. Christandl, A. Ekert, B.-G. Englert, D. Kaszlikowski, and C. Macchiavello, Phys. Rev. Lett. **91**, 097901 (2003).
[15] Y. C. Liang, D. Kaszlikowski, B.-G. Englert, L. C. Kwek, and C. H. Oh, Phys. Rev. A **68**, 022324 (2003).
[16] B.-G. Englert, D. Kaszlikowski, H. K. Ng, W. K. Chua, J. Řeháček, and J. Anders, e-print quant-ph/0412075.
[17] E. Andersson, S. M. Barnett, and A. Aspect, Phys. Rev. A **72**, 042104 (2005).
[18] R. Azzam, I. Elminyawi, and A. El-Saba, J. Opt. Soc. Am. A **5**, 681 (1988).
[19] In the language of spin-$\frac{1}{2}$ systems the reduced Stokes vector is the Pauli vector and the Poincare sphere is called the Bloch sphere.
[20] K. Kraus, *States, Effects and Operations. Fundamental Notions of Quantum Theory, Lecture Notes in Physics*, Vol. 190 (Springer-Verlag, Berlin, 1983).
[21] B.-G. Englert, K. M. Tin, C. G. Goh, and H. K. Ng, Laser Phys. **15**, 7 (2005).
[22] E. L. O'Neill, in *Introduction to Statistical Optics* (Dover, New York, 1991), Chap. 9.
[23] R. M. A. Azzam and F. F. Sudrajat, Appl. Opt. **44**, 190 (2005).
[24] C. Kurtsiefer, M. Oberparleiter, and H. Weinfurter, Phys. Rev. A **64**, 023802 (2001).
[25] A. Uhlmann, Rep. Math. Phys. **9**, 273 (1976).
[26] R. Jozsa, J. Mod. Opt. **41**, 2315 (1994).
[27] S. Gaertner, H. Weinfurter, and C. Kurtsiefer, Rev. Sci. Instrum. **76**, 123108 (2005).